DOI: 10.1002/ejoc.200900850

# Synthesis and Optical and Electronic Properties of Thiophene Derivatives

**Raphael P. Jimenez,[a] Masood Parvez,[a] Todd C. Sutherland,*[a] and Joel Viccars[a]**

**Keywords:** Structure-activity relationships / Heterocycles / Chromophores / Electrochemistry / Density functional calculations

Using the Hinsberg synthesis of thiophenes, a versatile method to prepare fully derivatized, π-extended thiophenes is reported. Functionalized thiophenes were divergently synthesized to create three classes of compounds – electron-deficient, extended conjugation and electron-rich – to assess substituent effects on optical and electrochemical properties. Properties were assessed by solution absorption spectroscopy, solution- and solid-state fluorescence spectroscopy, cyclic voltammetry and density functional theory calculations. Tetracyano derivatives, prepared through Knoevenagel condensations of malononitrile with thiophene-2,5-dicarbaldehydes, were used as electron-poor analogs. These derivatives showed quasireversible reduction reactions and very low-lying calculated LUMO energies (–0.55 V reduction potentials vs. $Fc/Fc^+$). The effect of extending π conjugation on the optical and electrochemical properties was investigated by the installation of bis(2-thienylacryonitrile) groups onto three thiophene cores. The extended conjugation led to compounds that demonstrated both solution- and solid-state fluorescence and moderate, irreversible reduction potentials (–1.2 V versus $Fc/Fc^+$). The Lewis-acid-catalyzed coupling of four indoles to thiophene-2,5-dicarbaldehydes was studied to assess the effects of both electron-donating substituents and a quinoidal thiophene. The tetraindolic thiophenes possessed low HOMO–LUMO energy gaps of 1.91 eV, high-lying HOMO energy levels and tunable LUMO energy levels, attributed to the thiophene quinoidal ground-state structure.


## Introduction

Interest in organic electronics has grown significantly over the past several decades. Research has focused on improving material processability, stability and performance.[1–7] Today, thiophene-based materials show applications in organic field-effect transistors (OFETs),[8–12] organic light-emitting diodes (OLEDs),[13,14] conducting polymers[15–17] and organic photovoltaic devices.[18–20] More recently, efforts in developing and optimizing materials useful for optoelectronics has increased due to the need for solar energy conversion materials.[21] Near-IR absorption[22,23] as well as band-gap tunability[6,19,24–28] are key features needed for such materials. The ubiquitous use of thiophene in organic materials is in part due to its electronic properties, ease of derivatisation and commercial availability.

The synthesis of new molecules that have small HOMO–LUMO energy differences is paramount to advancing organic materials applications. Moreover, the synthesis should also be scalable, efficient, modular and divergent to allow tuning of the electronic structure and solubility characteristics required for different materials applications. Two strategies are generally employed to decrease the HOMO–LUMO energy gap. The first strategy involves increasing the degree of conjugation by the introduction of more double bonds. The second strategy involves the incorporation of both an electron-donating group (EDG) and electron-withdrawing group (EWG) within the same molecule.[29] Small-molecule tuning, as opposed to a polymeric approach, permits well-defined structure-property relationships to be built in the absence of aggregate or supramolecular structures. Low-band-gap organics have been synthesized by Osuka and co-workers[30,31] using fused porphyrin tapes that demonstrate electronic transitions at energies as low as 0.45 eV. Unfortunately, due to low yields and poor solubility, these materials do not lend themselves to practical materials applications. Roncali and co-workers have synthesized a wide variety of thiophenes for use as organic semiconductors with tunable HOMO–LUMO energies.[32–34] Molecules with small HOMO–LUMO energy differences can also be obtained by the installation of an electron-donating (increasing the HOMO energy) moiety and an electron-accepting (lowering the LUMO energy) moiety into a single molecule.[29] However, the frontier molecular orbitals (FMOs) of these donor-acceptor (D-A) dyads are localized on the respective electron-rich and electron-poor regions of the molecule, often resulting in poor overlap and weaker electronic transitions. Nevertheless, small molecules with low HOMO–LUMO energy differences have been synthesized using the D-A approach.[35]

[a] Department of Chemistry, University of Calgary,
2500 University Drive NW, Canada
Fax: +1-403-289-9488
E-mail: todd.sutherland@ucalgary.ca
Supporting information for this article is available on the WWW under http://dx.doi.org/10.1002/ejoc.200900850 or from the author.

  

There is a clear need for new organic compounds that have tunable electronic and optical properties. This contribution explores an efficient route to synthesize thiophenes with the potential for different functionalities at the ring positions, as shown in Scheme 1. This contribution is divided into two parts: first, the synthesis and optical and electronic characterisation of a series of thiophene cores and second, the divergent modification of those thiophene cores into classes of electronically diverse derivatives. For the first part, the Hinsberg thiophene synthesis was employed, which resulted in three fully derivatised thiophene structures in moderate yields after a simple purification. For the second part, the three thiophene cores were modified by the installation of either EWGs, π-extension groups or EDGs to create a tunable family of thiophene derivatives.

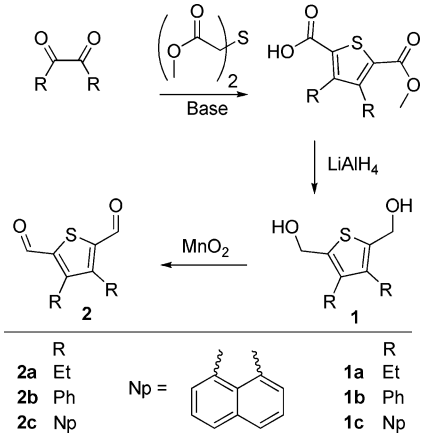


Scheme 1. Hinsberg synthesis of **1a**–**c** and **2a**–**c** with a thiophene core.

## Results and Discussion

The Hinsberg thiophene synthesis[36] starts with the condensation of dimethyl 2,2′-thiodiacetate with an α-diketone in the presence of base to produce thiophene,[37] as shown in Scheme 1. During the Hinsberg reaction, the 2- and 5-positions of thiophene become differentiated resulting in an asymmetrical, substituted thiophene (2-acid-5-ester) from symmetric starting materials. We did not exploit the asymmetry. Instead, we reduced the 2-acid-5-ester-thiophenes to the symmetric thiophene-2,5-dimethanols, shown as series **1**. Related thiophene-2,5-dimethanols have been synthesized previously,[38–40] and the synthesis of **1b** has been reported by Nakayama[41] and Chandra.[42] We gently oxidized series **1** using $MnO_2$[43] to yield thiophene-2,5-dicarbaldehydes, series **2**, in nearly quantitative yields. Several thiophene-2,5-dicarbaldehyde examples[39,44–50] have been synthesized over the last twenty years, including fused aromatics thiophenes. Specifically, the synthesis of **2b** has been previously reported.[41,42] The conversion of the thiophene-dimethanol derivatives to their corresponding dicarbaldehydes (series **2**) explores the electronic effects of EDGs and EWGs at the 2,5-loci of thiophene. In addition, the aldehyde functionality is a reactive handle for a variety of coupling reactions, such as acid-catalyzed aromatic substitution or a variety of carbanion couplings, which are demonstrated later in this contribution.

Symmetric α-diketones were used to furnish the 3,4-thiophene substituents. We investigated a family of diketones to cover a range of electronic tuning from alkyl (**a**) to phenyl (**b**) to fused naphthyl (**c**). In order to develop structure-function relationships, we needed a thorough understanding of the electronic properties of **1a**–**c** (thiophene-diols) and **2a**–**c** (thiophene-dicarbaldehydes) before synthetically modifying the core thiophene structure. We examined both series **1** and **2** by cyclic voltammetry (CV), UV/Vis and density functional theory (DFT) calculations to provide the basis for comparison with further derivatisation.

We crystallised the three thiophene-dicarbaldehydes (series **2**) as well as thiophene-dimethanol **1b** from a ternary solvent of methanol, dichloromethane and toluene (10:10:1), yielding crystals of X-ray quality. ORTEP images (at 50% probability) of each are shown in Figure 1. Comparisons with available crystal data (CCDC) of neutral tetrasubstituted thiophenes show typical bond lengths and angles, which are included in the Supporting Information.

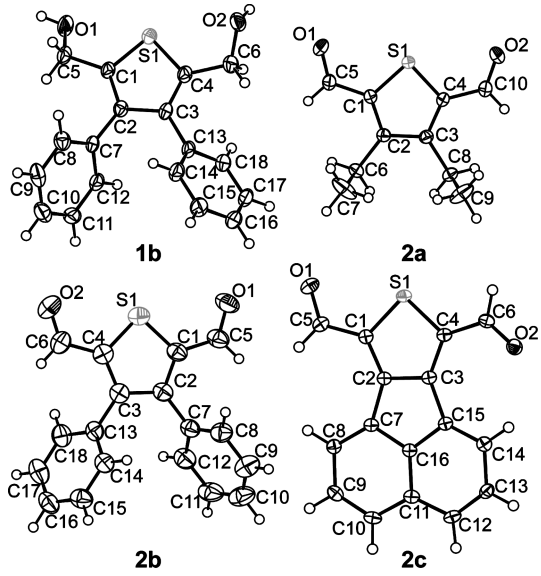


Figure 1. ORTEP represenatations of **1b** and **2a**–**c** at 50% probabilities.

We used the single-crystal-determined geometries (for **1b** and **2a**–**c**) as the geometry input files for DFT calculations. A comparison of crystal geometries with optimized DFT structures [using the B3LYP functional with the 6-31+G(d,p) basis set] revealed very good agreement, with the exception of **2a**, where the crystal structure had both 3,4-ethyl pendant groups in a *cis* orientation, which we attributed to a solid-state packing phenomena. The agreement of the crystal data with optimized structures gave credibility to the optimized structures where crystal data is not available.

  

We carried out nucleus-independent chemical shift (NICS) calculations[51,52] to assess the aromaticity of the thiophene ring using GIAO-SCF at the HF/6-31G+(d,p) level with the GAUSSIAN 03 software package[53] (see the Supporting Information). The objective of the NICS(1) calculations was to correlate the effects of aromaticity of the thiophene core on its optical and redox properties. The NICS(1) values of series **1** showed decreasing aromatic character from –11.5 to –8.34 to –7.61 for **1a** to **1c**, respectively. We observed a similar decreasing aromatic trend for series **2** with NICS(1) values of –10.26, –9.04 and –8.56 for **2a** to **2c**, respectively. The decrease in aromaticity for both series, from the diethyl-thiophene to the acenaphthyl (AcNp)-thiophene derivatives, was consistent with the thiophene ring delocalizing its π-system to the 3,4 aromatic substituents (extension of the αC–S bonds and contraction of the fused aromatic σ bonds). The solid-state packing diagrams of **1b** and **2a**–**c** are included in the Supporting Information.

The UV/Vis absorption spectra of series **2** are shown in Figure 2, and as expected, the more π-delocalized thiophene structures showed red-shifted absorptions.[29,54] The onset of the absorption, used to determine the HOMO–LUMO energy gap, of the molecule is included in Table 1. Within both series **1** and **2**, the HOMO–LUMO energy gap decreased progressing from the diethyl (**a**) to diphenyl (**b**) to AcNp (**c**) thiophenes. The decrease in the HOMO–LUMO energy gap we attributed to increased conjugation, which was supported by DFT calculations. The UV/Vis absorption spectra also showed series **2** had a consistently lower HOMO–LUMO gap than its thiophene-2,5-dimethanol precursor. We note the calculated HOMO–LUMO energies are gas-phase calculations and should be considered as verifying a trend in energies rather than matching experimental values. Neither series **1** nor **2** were fluorescent in solution (THF) or the solid state.

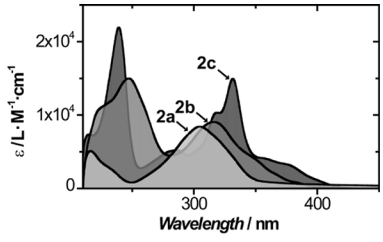


Figure 2. UV/Vis spectra of **2a**–**c** in THF.

The CV results are compiled in Table 1. Generally, series **1** showed two irreversible oxidation waves. The first oxidation wave we attributed to the one-electron oxidation of thiophene (1.0 V to 1.2 V) to the radical cation, which becomes less energetic with increased conjugation.[55,56] The oxidation of thiophenes is known to be irreversible and fall within the reported potential region.[57] The second irreversible oxidation wave, which was at similar potentials throughout series **1**, we attributed to the alcohol oxidation (about 1.5 V).

Compounds **1a** and **1b** did not show reduction peaks within the solvent stability window, whereas **1c** showed two quasireversible reduction waves at –1.43 V ($\Delta E_p$ = 110 mV) and –1.89 V ($\Delta E_p$ = 110 mV). The two quasireversible reduction waves we tentatively assigned to the radical anion and dianion delocalized over the entire molecule,[58,59] as suggested by the LUMO of **1c**. Spectroelectrochemical experiments are ongoing to determine the identity of the reduced species. A trend in series **1** of decreasing oxidation potential (from **1a** to **1c**) was consistent with optical measurements and DFT calculations. The thiophene-dicarbaldehydes (series **2**) did not exhibit a second oxidation wave, which supports the alcohol oxidation assignment made for series **1**. The first irreversible oxidation waves of **2a**–**c** occurred at similar or lower values than those of series **1**, suggesting the small effect that EDGs or EWGs in the thiophene α-positions have on the HOMO levels of thiophenes. All of series **2** showed two quasireversible reduction waves. Compound **2a** had the highest reduction potential at –1.75 V ($\Delta E_p$ = 700 mV) and –2.5 V ($\Delta E_p$ = 650 mV), whereas **2b** ($\Delta E_p$ = 250 mV) and **2c** ($\Delta E_p$ = 560 mV) had their first reduction potentials at –1.5 V. The two reduction waves of series **2** we attributed to the radical anion and dianion species.

The energy levels of the FMOs for series **1** and **2** are shown in Figure 3. Two trends are apparent. First, the HOMO energy levels increased from **a** to **c** in both series **1** and **2**. Second, the electron-rich 2,5-dimethanol derivatives (**1**) had higher energy lying HOMO and LUMO levels than does series **2**. Both 3,4-diethylthiophenes (**1a** and **2a**) had HOMOs confined to the thiophene ring, whereas the 3,4-diphenylthiophenes and AcNp-thiophene (**1b**, **1c**, **2b** and **2c**) showed π-delocalization onto the 3,4-thiophene substituents, suggesting potential tuning. All FMO images are available in the Supporting Information. The HOMO energy level changes for both series **1** and **2** were consistent with the observed first oxidation wave measured by CV.

Table 1. Electrochemical and optical data of **1a**–**c** and **2a**–**c**.

| Entry | Compound | Absorbance onset [nm] (eV) | $E_{ox1}$ [V] | $E_{ox2}$ [V] | $E_{red1}$ V | $E_{red2}$ [V] | Calculated HOMO–LUMO [eV][c] |
|---|---|---|---|---|---|---|---|
| 1 | **1a**[a] | 309 (4.01) | 1.13 | 1.50 | –[d] | –[d] | 5.95 |
| 2 | **1b**[a] | 294 (4.21) | 1.19 | 1.56 | –[d] | –[d] | 5.08 |
| 3 | **1c**[a] | 399 (3.11) | 1.01 | 1.44 | –1.43 | –1.89 | 4.03 |
| 4 | **2a**[b] | 354 (3.50) | 1.13 | – | –1.75 | –2.47 | 5.25 |
| 5 | **2b**[b] | 398 (3.11) | 1.15 | – | –1.54 | –2.02 | 3.90 |
| 6 | **2c**[b] | 423 (2.93) | 0.85 | – | –1.59 | –2.17 | 3.44 |

[a] Measurements were conducted in $CH_3CN$. [b] Measurements in THF; scan rate of 0.1 V $s^{-1}$; concentration of 1.0 mM; tetrabutylammonium hexafluorophosphate (0.1 M) was the supporting electrolyte vs. an $Fc/Fc^+$ reference. [c] Calculated by the DFT B3LYP functional with the 6-31+G(d,p) basis set. [d] Not observed within the potential window of the solvent.

  

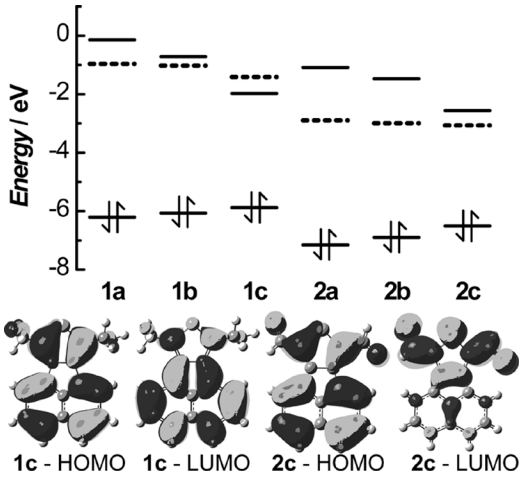


Figure 3. FMO energy levels calculations [DFT B3LYP functional and 6-31G+(d,p) basis set] for series **1** and **2**. Quinoidal-shaped LUMO orbitals are indicated by the dashed line.

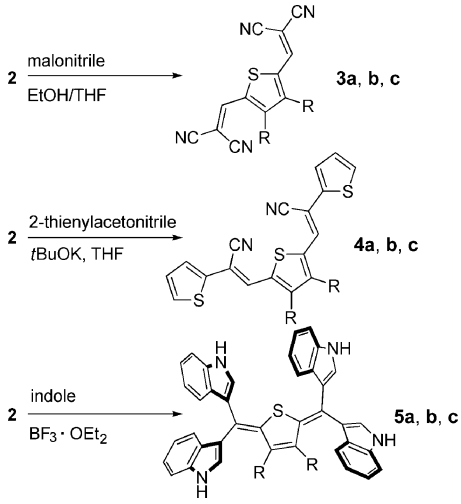


Scheme 2. Synthesis of tetracyano-thiophene (**3**), dithienyldicyano-thiophene (**4**) and tetraindole-thiophene (**5**).

The LUMOs of all compounds except for **1c** had the expected quinoidal thiophene shape[60] with density on the thiophene ring, as exemplified by **2c**-LUMO in Figure 3. The energy levels of the quinoidal LUMOs changed slightly for **2a**–**2c**, which was consistent with the small changes observed in the first reduction. Interestingly, the LUMO+1 of **2c** did show a significant decrease in energy compared to the LUMO+1 of both **2a** and **2b**. This drop in energy is critical for the tunability of these fused aromatic compounds. However, in the AcNp-thiophene (**1c**) case, the LUMO energy dropped below the quinoidal orbital (now LUMO+1), showing the potential for extensive LUMO tunability using fused aromatic thiophenes. The DFT calculations indicated the installation of EDGs at the 2,5-loci of thiophene allow for LUMO energy-level tuning, and the fused aromatics at the 3,4-loci permit HOMO energy level tuning.

With a thorough characterisation of the optical and electronic properties of the thiophene core, we synthesized three divergent families of compounds from series **2**. Scheme 2 illustrates the synthetic versatility of the thiophene core, which is conducive to the addition of electron-withdrawing cyano groups by Knoevenagel condensations (series **3**), the extension of conjugation via bis(2-thienylacrylonitrile)-thiophene derivatives (series **4**) and the formation of a tetraindolic thiophenes (series **5**).

We carried out the Knoevenagel condensations of thiophene-2,5-dicarbaldehydes **2** with malononitrile in EtOH/THF with gentle heating, resulting in 67–72% conversions to the tetracyano-thiophenes (series **3**) within 25 min. We purified each of the series **3** compounds by crystallisation, and their UV/Vis absorption spectra are included in the Supporting Information. The installation of the four cyano groups onto the divinyl thiophene core resulted in a bathochromic absorption relative to series **2**. Both structures **3a** and **3b** had absorption onsets of about 450 nm, which were shifted 100 nm from **2a** and 50 nm from **2b**. Clearly, the replacement of the 3,4-diethyl groups with the 3,4-diphenyl groups did not impact the HOMO–LUMO energy gap. DFT calculations resulted in a HOMO–LUMO energy gap of 2.93 eV and 2.95 eV for **3a** and **3b**, respectively, which was consistent with the optically determined HOMO–LUMO energy gap. As expected, the strong EWGs had lowered the LUMO energy level by about 1.1 eV compared to that of series **2**. The large change observed in the LUMO energy level resulted in a modest (0–0.3 eV) decrease in the HOMO energy level. Compound **3c** exhibited a larger 100 nm bathochromic shift in its absorption onset (525 nm) compared to that of its series **2** parent. The acenaphtho-fused aromatic thiophene (**3c**) exhibited delocalization of the π-system through the 3,4-positions, which did not occur in either the diethyl (**3a**) or diphenyl (**3b**) cases. A similar compound (R = H in Scheme 2), was first reported by Sone[61] and was later investigated as an electron-acceptor material.[62] In addition, a 3,4-benzannulated analogue of **3a** was synthesized previously[62] and showed two reversible reduction waves at –0.25 V and –0.62 V (vs. Ag|AgCl).[62] The addition of the four cyano groups in series **3** resulted in bathochromic shifts, and we observed insignificant changes in molar absorptivity, suggesting the cyano groups did not extend the π-conjugation but rather lowered the LUMO energy level inductively. Only **3c** possessed weakly emissive properties in THF with a $\lambda_{em}$ maximum at 544 nm ($\lambda_{ex}$ = 490 nm). The excitation spectrum peaked at 490 nm, consistent with the absorption spectrum, corresponding to a moderate Stokes shift of 53 nm. NICS(1) calculations for **3a**–**c** showed a decrease in thiophene aromatic character with values of –9.98, –9.85 and –7.86, respectively, consistent with the trends observed for series **2**. NICS(1) results indicated that better chromophores based on thiophene cores should possess less aromatic thiophenes. Interestingly, both **3a** and **3b** were weakly emissive in the solid state. Single crystal X-ray structures of **3a** and **3b** showed antiparallel stacking of the thiophene groups with little π-overlap (see the Supporting Information). The solid-state excitation spectra of **3a** and **3b** overlapped with

  

their absorption spectra, suggesting the solid-state packing did not involve donor-acceptor orbital mixing. Instead, the solid-state packing confined the thiophene and limited other relaxation pathways, resulting in a weakly emissive solid at similar energy to solution fluorescence.

The CVs of series **3** are included in the Supporting Information. Generally, we reduced the tetracyano-thiophene derivatives easily at moderate potentials (–0.55 V vs. $Fc/Fc^+$, see Table 2.) Compound **3a** showed irreversible reduction, whereas both **3b** and **3c** showed quasireversible behaviour under the same conditions, as shown in Figure 4. The quasireversible CV peaks were most likely the radical anion that has been observed previously.[63] We note that we did not observe quasireversible behaviour when the reversal potential was more negative than –0.6 V (–1.1 V vs. $Fc/Fc^+$) because further reduction created a new, coloured species, which we observed diffusing from the electrode surface. At this time, the identity of the reactive species in unknown, but we observed the subsequent oxidation of the new species in the return wave at potentials near 0 V. We did not observe the oxidation peak above 0 V in the first anodic scan, and it only appeared on subsequent scans after we applied reduction potentials more negative than –0.6 V. In a cathodic potential sweep experiment, the potential where the current begins to increase is termed the onset of reduction and provides an estimate of the LUMO energy level. Based on the CV data, we observed no discernible differences in LUMO energy levels for series **3**, which was supported by DFT calculations (discussed below). Similarly, the HOMO energy levels can be evaluated electrochemically by the onset of oxidation, but in the tetracyano derivatives, this oxidation potential resided outside the solvent stability window. The low reduction potentials of **3b** and **3c** indicated the possible use of this class of thiophene as *n*-type organic materials. The quasireversible CVs of **3b** and **3c**, shown in Figure 4, suggested the stability of the reduced species was enhanced by the introduction of the four cyano groups and could play a role in eventual device longevity. Moreover, the kinetics of the electron-transfer reactions, as assessed by the oxidation and reduction peak separation, indicated **3c** ($\Delta E_p$ = 80 mV) was operating near diffusion-controlled limits, in contrast to **3b** ($\Delta E_p$ = 260 mV), and could lead to materials with superior charge-transfer rates.

We synthesized series **4** from the condensation of 2-thienylacetonitrile with series **2** in the presence of *tert*-butoxide. The conversion to the bis(2-thienylacrylonitrile)-thiophene was nearly quantitative with yields ranging from 91–97% in a 30 min reaction. Both Roncali et al.[64] and Hanack et al.[65] have synthesized the 3,4-proton version of **4a**, which showed a $\lambda_{max}$ value at 480 nm in $CH_2Cl_2$ and reversible oxidation and reduction waves. In addition, electrochemical anodic polymerization of the protonated derivative produced a polymer film with a band-gap of 0.65 eV. A related, conjugated, donor-acceptor derivative[66] of bis(2-pyrrol-acryolnitrile)-thiophene showed oxidation at 0.48 V (vs. Ag|0.1 M $AgClO_4$, $CH_3CN$) and $\lambda_{max}$ at 490 nm, which was also electropolymerised and produced a polymer with a band-gap of 1.6 eV. The UV/Vis spectra of series **4** are included in the Supporting Information. Series **4** showed bathochromic absorptions compared to its parent dialdehyde. The absorption onsets for **4a**, **4b** and **4c** were 525, 525 and 550 nm, respectively. In addition, the absorption profiles of **4a** and **4b** in the low-energy region were nearly superimposable, indicating little electronic tuning of the HOMO or LUMO occurred due to substitution at the 3,4-positions of phenyl for ethyl. Fusion of an acenaphthylene ring to the thiophene core allowed the 3,4-loci to participate in π-delocalization, resulting in lower-energy electronic transitions. The lower-energy absorption onset of series **4** compared to series **3** was due to the additional conjugation length, consistent with the increase in molar absorptivity from $2 \times 10^4$ to $3 \times 10^4$ $M^{-1} cm^{-1}$. DFT calculations of series **4** indicated the HOMO–LUMO energy gaps were mainly dependent on HOMO-level tuning. The LUMO energy levels of series **4** were similar in energy to those of its parent series **2** dialdehydes, despite the introduction of the acrylonitrile group.

Table 2. Summary of electrochemical[a] and optical[b] data for series **3**–**5**.

| Entry | | $E_{red2}$ [V] | $E_{red1}$ [V] | $E_{ox1}$ [V] | $E_{ox2}$ [V] | Optical $E_g$ [eV][b] |
|---|---|---|---|---|---|---|
| 1 | **3a** | –1.22 | –0.59 | NA | NA | 2.58 |
| 2 | **3b** | –1.11 | –0.54 | NA | NA | 2.61 |
| 3 | **3c** | –0.99 | –0.69 | NA | NA | 2.36 |
| 4 | **4a** | –1.84 | –1.29 | NA | NA | 2.36 |
| 5 | **4b** | NA | –1.26 | NA | NA | 2.36 |
| 6 | **4c** | NA | –1.10 | NA | NA | 2.25 |
| 7 | **5a** | NA | NA | NA | NA | 2.07 |
| 8 | **5b** | NA | NA | NA | NA | 2.07 |
| 9 | **5c** | NA | NA | 1.63 | NA | 1.91 |

[a] All electrochemical measurements were conducted in 0.1 M $NBu_4PF_6$ as the supporting electrolyte in THF at a scan rate of 0.1 $V s^{-1}$, using a Pt wire working electrode vs. A $Fc/Fc^+$ reference. [b] The optical band gap was determined from the onset of absorption in $1 \times 10^{-5}$ M THF solutions.

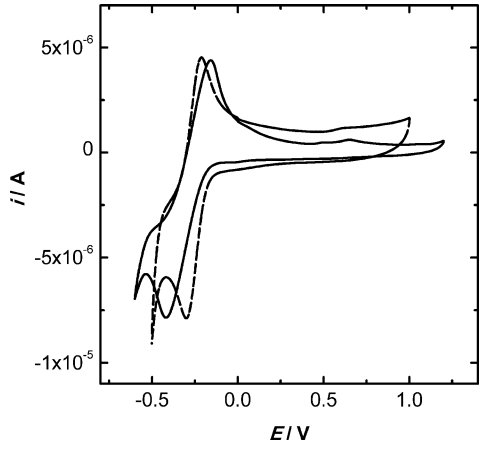


Figure 4. CVs of **3b** (solid line) and **3c** (dashed line) in THF at room temperature; scan rate of 0.1 $V s^{-1}$; concentration of 1.0 mM; tetrabutylammonium hexafluorophosphate (0.1 M) was the supporting electrolyte; reference electrode of $Ag|AgCl|KCl_{3M}$; a Pt wire as the working electrode and a Pt mesh as the counter electrode.

  

The electron-withdrawing cyano groups did not alter the LUMO energy level because the electronics were compensated by the electron-rich thienyl groups. However, the thienyl substituents, due to extended π-conjugation, increased the HOMO energy level by 0.9–1.3 eV. The results of the DFT calculations on series **4** clearly indicated the thienyl groups donated significant electron density into the conjugated π-backbone. NICS(1) calculations resulted in less thiophene aromatic character than series **3** with **4a**–**c** having values of –9.82, –8.22 and –7.32, respectively, which was consistent with the notion of extended conjugation.

Both **4b** and **4c** were fluorescent as dilute THF solutions with emission peaks at 520 and 540 nm, respectively, and small Stokes shifts of 25 and 20 nm, respectively. All of series **4** exhibited solid-state fluorescence. Notably, **4b** showed a solid-state fluorescence that was red-shifted compared to its solution-based fluorescence. The solid-state emission maxima for **4a** and **4b** were 580 and 675 nm, respectively. An X-ray structure for **4a** (Figure 5) showed stacking of the π-extended thiophenes with a distance between thiophene ring planes of 3.47 Å, which could lead to intermolecular π-π interactions and orbital mixing, resulting in lower energy electronic transitions. A similar structure and packing motif was reported by Wagner et al.[67] Presumably, similar packing could explain the bathochromic solid-state emission spectrum of **4b**, but a single crystal is not yet available. The overlap of π-orbitals in the solid-state packing of **4a** is clearly visible in parts b and c of Figure 5, in contrast to the limited degree of π-orbital overlap seen in the solid-state packing of **3a** or **3b** (see the Supporting Information). The solid-state emission spectrum of **4c** did not follow the solution-based absorption and emission trend with an emissive peak at 590 nm. Most likely, the solid-state structure of **4c** did not provide effective intermolecular overlap of the π-systems, resulting in an emissive peak that was only 40 nm red-shifted compared to its solution fluorescent peak.

The CVs of series **4** are included in the Supporting Information. None of series **4** showed reversible redox behaviour, and the onsets of reduction were shifted cathodically compared to series **3**, due to the two electron-rich thienyl substituents. The addition of electron density to the system resulted in an increase in LUMO energy. Both **4a** and **4b** showed the same reduction onset potentials, which were in agreement with the DFT-determined LUMO energy levels, and **4c** was slightly easier to reduce, which was also consistent with DFT calculations. The oxidation peaks of the first anodic scan, to determine HOMO energy levels, were outside the stability window of the solvent. However, upon subsequent CV scans, we observed two oxidation peaks in the CV between 0 V and 1 V that we attributed to a highly coloured, oligomeric species observed with related bis(thienylvinyl)thiophenes formed during the reductive cycle.[59,65] On the first anodic scan of a clean electrode, the oxidation peaks between 0 and 1 V were absent, and after several cycles, we did not observe any visible film on the electrode surface owing to the solubility of the oligomeric species in THF.

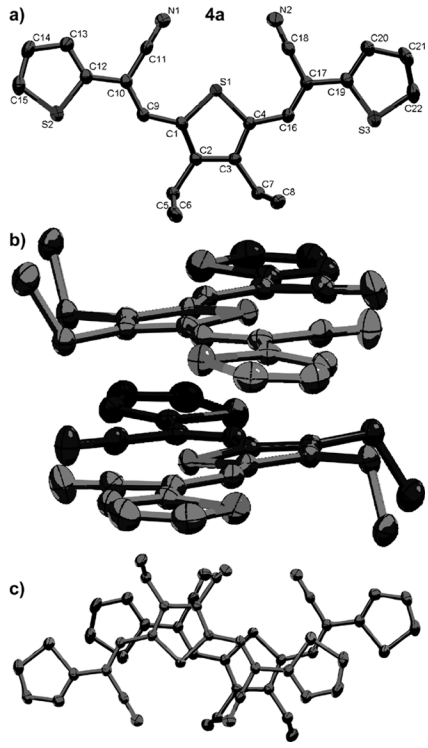


Figure 5. a) Ortep representation of **4a** shown at the 50% probability level. b) side view of solid-state packing; c) top view of solid-state packing.

We synthesized series **5** using the Lewis-acid-catalyzed reaction of the dialdehyde (series **2**) with indole, resulting in moderate yields of 41–49%. The conversion took longer than for either series **3** or **4**, and column chromatography was required to purify the final products. The $^1$H NMR of **5a** was unique because it showed two conformations of the 3,4-diethyl groups – *syn* and *anti* – at room temperature. Variable-temperature $^1$H NMR spectra (see the Supporting Information) showed the convergence of the $C_2$-symmetric *anti* conformer into the thermodynamically preferred, asymmetric *syn* conformer. We established the assignment of the two conformers using COSY and NOESY experiments (see the Supporting Information) and DFT calculations. The asymmetric *syn* diethyl conformer was more stable than the *anti* diethyl conformer by 5 kJ mol$^{-1}$ [calculated value using the B3LYP functional with the 6-31 G+(d,p) basis set]. The two diethyl conformations and $^1$H NMR assignments are available in the Supporting Information. The UV/Vis spectra of series **5** are shown in Figure 6. We observed the same overall trends as we did for series **3** and **4**, with the diethyl and diphenyl derivatives having nearly overlapping spectral features in the low-energy region. The absorption spectrum of **5c** was unique because of its lower molar absorptivity and broad transitions, which could be attributed to the different conformations present at room temperature. However, series **5** did exhibit the largest bathochromic shifts of all the series, which we ascribed to the extensive delocalization of the π-system and the quinoidal thiophene ground-state structure. The ab-

  

sorption onsets of **5a**–**c** were 600, 600 and 650 nm, respectively. For comparison, quinoidal thiophenes synthesized by Hanack et al.[65,68–71] bearing bis(2-thienyl)thiophene with 3,4-annulated phenyl and thiophene groups showed absorbance maxima at 432 and 405 nm, respectively. Additionally, non-annulated, quinoidal, terthiophenes showed an absorbance maximum at 554 nm.[70] Lorcy et al. synthesized tetracyano, benzannulated, quinoidal thiophenes, which gave an absorption maximum at 408 nm.[62] Ishii et al. synthesized several 2,5-bis(diarylmethylene)thiophenes that exhibited absorbance maxima from 414 to 527 nm in $CH_3CN$.[72] An interesting set of quinoidal tetraazulene-thiophenes by Ito et al.[73] and Takekuma et al.[74] had absorbance peaks at 530 and 550 nm, respectively.

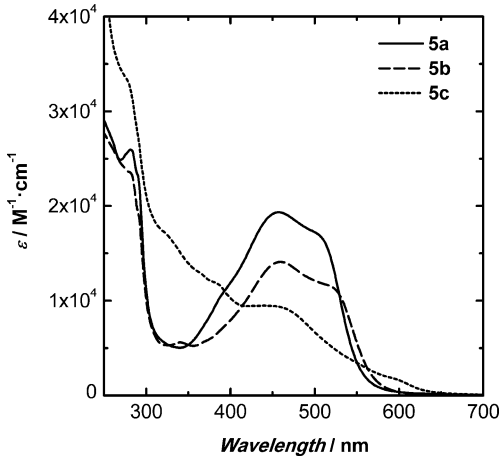


Figure 6. UV/Vis spectra of series **5** in THF.

DFT calculations revealed that the HOMO energy levels for series **5** increased substantially (2.2–2.8 eV) from those of the parent dialdehydes, series **2**. We observed a concurrent increase in LUMO energy level (compared to series **2**), but at a much smaller magnitude (0.8–1.3 eV), resulting in an overall smaller energy gap. NICS(1) calculations clearly demonstrated a quinoidal (nonaromatic) form of thiophene with values of –2.97, –1.47 and –1.50 for **5a**–**c**, respectively. Only **5b** and **5c** displayed fluorescent behaviour as dilute THF solutions, and these data are included in the Supporting Information. The excitation spectrum of **5b** aligned with the absorption spectrum shown in Figure 6 and had an emission peak at 570 nm. The excitation spectrum of **5c** was very different from the **5c** absorption spectrum shown in Figure 6. The **5c** excitation spectrum peaked at 340 nm and emitted at 415 nm, clearly blue-shifted from the absorption spectrum. Excitations at the absorption shoulders of 600 nm or 460 nm for **5c** did not result in emissive transitions, whereas photoexcitation of the shoulder at 340 nm resulted in emission at 415 nm. This blue-shifted emission we attributed to one of the indoles relaxing. Due to lack of solubility, the CVs of series **5** were not informative. The DFT-determined LUMO energy levels for the tetraindoles showed a decreasing energy trend across the diethyl (**5a**) to diphenyl (**5b**) to acenaphtho-fused (**5c**) derivatives.

The cumulative results of the DFT gas-phase calculations with the B3LYP/6-31G+(d,p) basis set are shown in Figure 7. Series **3**, with the four cyano groups, possessed the lowest energy LUMOs and highest energy HOMOs and was the easiest to reduce. Series **4**, with the added electron density of the pendant thienyl groups, had both a higher energy HOMO and LUMO than those of series **3**. Series **5** showed an increase in HOMO energy over that of series **4**, concurrent with an increase in LUMO energy. Within series **3**, it was clear that the LUMO energy was not altered or tunable by changes to the 3,4-loci of the thiophene.

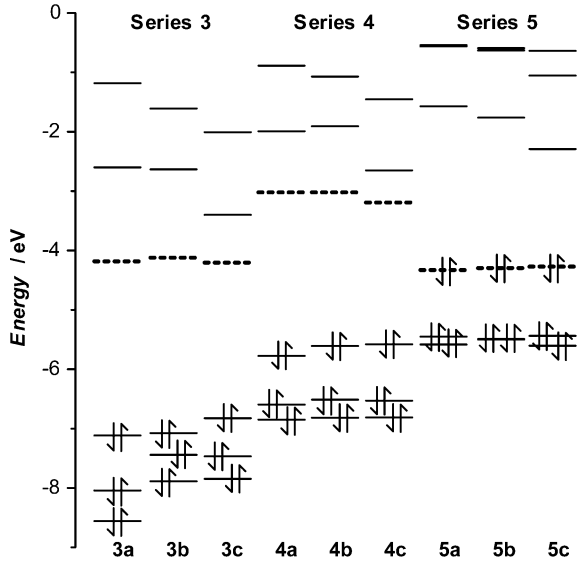


Figure 7. FMOs of series **3**–**5**, determined with the DFT B3LYP functional and the 6-31G+(d,p) basis set. Quinoidal-shaped orbitals are indicated by the dashed line.

However, the HOMO energy of the fused acenaphtho derivative, **3c**, did show tunability potential, as seen by the **3c**-HOMO surface shown in Figure 8. The **3c** HOMO surface did indicate much electron density was delocalized over the naphthalene ring, an effect not repeated with either the diphenyl (**3b**) or diethyl (**3a**) derivatives (see the Supporting Information for FMOs). Within series **4**, only moderate changes of either the HOMO or LUMO energy levels were apparent. The largest changes in series **4** stemmed from the LUMO lowering of the fused acenaphtho derivative, **4c**, attributed to the small delocalization onto the naphthalene ring in the LUMO surface. Within series **5**, the HOMO energy level remained constant. Importantly, the HOMO surface for all of series **5** changed to a quinoidal shape, as shown in Figure 8, with the majority of electron density residing on the thiophene ring and limited density spread over the heterocycle of the indole. The quinoidal HOMO orbital did not include contributions from the 3,4-loci and, therefore, the energy remained constant across the series. However, the LUMO energy of series **5** was highly tunable by the 3,4-loci of thiophene. The LUMO of the diethyl derivative, **5a**, showed no contribution on the ethyl pendants,

  

whereas both the diphenyl (**5b**) and fused acenaphtho (**5c**) derivatives showed delocalization through the 3,4-thiophene positions, concurrent with a stepwise reduction in LUMO energy level.

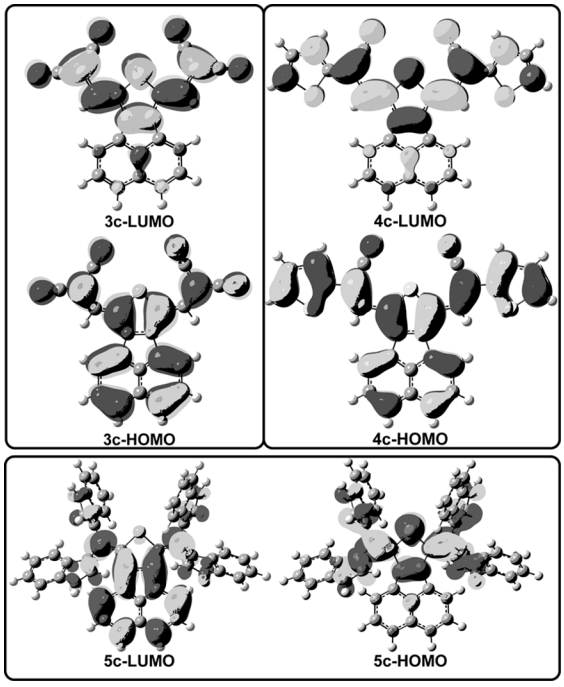


Figure 8. DFT-calculated HOMO–LUMO surfaces for **3c**, **4c** and **5c**.

## Conclusions

In summary, this contribution details a facile Hinsberg synthesis of thiophene-2,5-dicarbaldehyde with ethyl, phenyl and naphthaleno-bridge substituents at the 3,4-thiophene positions. These thiophene-dialdehydes were subjected to three reactions to illustrate the tunability of the electronic energy levels. The Knoevenagel condensation with malononitrile resulted in high conversions into very electron-deficient thiophenes, which were reduced readily and exhibited weak solid-state emissions. The addition of two thienyl substituents and two cyano groups resulted in extended conjugation with little change in the HOMO energy level compared to that of its parent dialdehyde. However, the enhanced conjugation led to a large bathochromic shift and a solid-state fluorescence. The final series of syntheses was accomplished by the Lewis-acid-catalyzed reaction of indole with the parent dialdehyde resulting in a tetraindolic thiophene species. The tetraindolic species was more electron-rich than the other series studied and exhibited the lowest HOMO–LUMO gap. In addition, the tetraindolic compounds possessed a quinoidal thiophene core. Each compound was subjected to DFT calculations with the B3LYP functional and 6-31G+(d,p) basis set, and the calculations support both the electrochemical and photophysical measurements. The experimental and theoretical calculations indicate that the derivatisation of the 2,5-positions of the thiophene causes large changes in both the HOMO and LUMO energy levels. Conversely, the derivatisation of the 3,4-positions of thiophene causes minor changes in the electronic structure. The results clearly indicate that the fused acenaphtho-thiophene has the smallest HOMO–LUMO energy gap, and quinoidal-shaped thiophene ground states are attractive targets for low-band-gap organic materials. A major limitation is poor solubility; however, employing the Hinsberg synthesis allows a modular approach to the installation of solubilising groups at the α-diketone stage while maintaining the desired electronic structure. We envisage a combination of structures **3c** and **5c** into a new material that could produce a theoretical band gap of 0.1 eV. The major findings of this paper are threefold: 1) the Hinsberg thiophene synthesis is a versatile, efficient method for incorporating different functionality into the 3,4-positions and provides a path to fused aromatic structures, 2) the Knoevenagel condensations of thiophene-2,5-dicarbaldehydes, to extend conjugation, can alter the electronic structure dramatically, depending on the number of EWGs and length of conjugation, and 3) the formation of a quinoidal-shaped ground-state thiophene structure is advantageous to designing molecules with small HOMO–LUMO energy gaps.

## Experimental Section

**General Methods:** All chemical reagents were obtained from Aldrich and used without further purification, except deuterated solvents for NMR spectra, which were from Cambridge Isotope Laboratories. High-resolution mass spectra (HR-MS) were collected using a Waters GCT Premier instrument. $^{1}H$ and $^{13}C$ NMR spectra were recorded with a Bruker DMX-300 MHz or a DRY-400 MHz spectrometer. Proton spectra were referenced to $CHCl_3$ ($\delta$ = 7.27 ppm) or DMSO ($\delta$ = 2.50 ppm) as an internal standard. All carbon NMR samples were proton-decoupled and referenced to $CDCl_3$ ($\delta$ = 77.00 ppm) or DMSO ($\delta$ = 39.51 ppm). The UV/Vis/NIR spectra were recorded with a Varian Cary 5000 photospectrometer in $CH_3CN$ at room temperature using a quartz 1 cm path length microcell. Infrared spectra were recorded with a Varian FTS-7000 FT-IR spectrometer in a KBr suspension operating in diffuse reflectance mode at room temperature. CVs were recorded in $CH_3CN$ or THF at room temperature: scan rate of 0.1 $V s^{-1}$; concentration of 1.0 mM; tetrabutylammonium hexafluorophosphate ($NBu_4^+$ $PF_6^-$, 0.1 M) as the supporting electrolyte; reference of Ag|AgCl|$KCl_{3M}$ using a Pt wire as the working electrode and a Pt mesh as the counter electrode. Fluorescence spectra were recorded with a Jasco FP6600 Spectrofluorimeter in THF at room temperature using a quartz 1 cm path length cell. Solid-state fluorescence samples were prepared by drop casting the compound from $10^{-5}$ M THF solutions onto a quartz window fixed at a 30° incident angle.

**1a:** 3,4-Diethyl-5-(methoxycarbonyl)thiophene-2-carboxylic acid (0.45 g, 1.87 mmol) was added to a solution of lithium aluminium hydride (0.18 g, 4.76 mmol) in THF (20 mL) at –78 °C. The grey solution was slowly warmed to room temperature and stirred overnight, at which point the solution was cooled to 0 °C, and water (0.5 mL) and aqueous NaOH (0.5 mL, 10%) were added slowly with frequent venting. The solution was then filtered to remove salts and insoluble particles. After recrystallisation from dichloro-

  

methane, colourless crystals weighing 0.083 g (21.0%) were obtained; m.p. 139–141 °C. $^1$H NMR (300 MHz, [D$_6$]DMSO): $\delta$ = 5.20 (t, $J$ = 5.47 Hz, 1 H, O$H$), 4.55 (d, $J$ = 5.46 Hz, 2 H, C$H_2$OH), 2.49 (q, $J$ = 7.5 Hz, 2 H, C$H_2$CH$_3$), 1.02 (t, $J$ = 7.53 Hz, 3 H, CH$_2$C$H_3$) ppm. $^{13}$C NMR (101 MHz, [D$_6$]DMSO): $\delta$ = 139.1, 137.3, 56.9, 20.0, 16.2 ppm. UV/Vis: $\lambda$ ($\varepsilon$, M$^{-1}$cm$^{-1}$) = 285 (210), 252 (4400) sh, 248 (4700) nm. IR: $\tilde{\nu}$ = 3340, 3267, 2742, 1990, 1442 cm$^{-1}$. LRMS (EI, 70 eV, $m/z$): 200 [M]$^+$. $C_{10}H_{16}O_2S$ (200.3): calcd. C 59.96, H 8.05; found C 59.60, H 8.02.

**1b:** 5-(Methoxycarbonyl)-3,4-diphenylthiophene-2-carboxylic acid (9.99 g, 28.3 mmol) was added to a solution of lithium aluminium hydride (2.61 g, 68.6 mmol) in THF (100 mL) at –78 °C. The grey solution was slowly warmed to room temperature and stirred overnight, at which point the solution was cooled to 0 °C, and water (1.0 mL) and aqueous NaOH (2 mL, 10%) were added slowly with frequent venting. The solution was then filtered to remove salts and insoluble particles. After recrystallisation from dichloromethane, a white solid was obtained, weighing 7.38 g (88%); m.p. 169–172 °C. $^1$H NMR (300 MHz, [D$_6$]DMSO): $\delta$ = 7.18 (m, 3 H), 6.96 (m, 2 H), 5.41 (t, $J$ = 5.40 Hz, 1 H, O$H$), 4.45 (d, $J$ = 5.41 Hz, 2 H, C$H_2$OH) ppm. $^{13}$C NMR (75 MHz, [D$_6$]DMSO): $\delta$ = 150.9, 143.2, 140.7, 136.1, 130.3, 128.3, 127.1, 57.6 ppm. UV/Vis: $\lambda$ ($\varepsilon$, M$^{-1}$cm$^{-1}$) = 275 (20400) sh, 266 (29300), 237 (61100), 212 (235000) nm. IR: $\tilde{\nu}$ = 3317, 3055, 2937, 1600, 1471 cm$^{-1}$. LRMS (EI, 70 eV, $m/z$): 296 [M]$^+$. $C_{18}H_{16}O_2S$ (296.4): calcd. C 72.94, H 5.44; found C 72.44, H 5.59.

**1c:** Acenaphthenequinone (6.0 g, 0.033 mol) and dimethyl 2,2′-thiodiacetate (6.74 g, 0.0378 mol) were dissolved in dry THF (175 mL) by warming the mixture to reflux. Sodium methoxide (4.085 g, 0.0756 mol) was added, and the solution was stirred under a N$_2$ atmosphere overnight. Aqueous HCl (0.1 M, 100 mL) was added to the dark red solution, and the mixture was stirred for an additional 30 min. The organic layer was extracted repeatedly with aqueous ammonium hydroxide (25%, 50 mL) until a sample of the aqueous layer gave no precipitate upon acidification. The combined aqueous layers were heated briefly to remove dissolved ether and acidified with concentrated HCl, yielding a crude brown solid, weighing 5.72 g. The crude acenaphtho[1,2-$c$]thiophene-7,9-dicarboxylic acid (5.55 g, 16.3 mmol) was added to a solution of lithium aluminium hydride (1.53 g, 40.2 mmol) in dry THF (100 mL) at –78 °C. The grey solution was slowly warmed to room temperature and stirred overnight, at which point the solution was cooled to 0 °C, and water (1.0 mL) and aqueous NaOH (2 mL, 10%) were added slowly with frequent venting. The solution was then filtered to remove salts and insoluble particles. After crystallisation from dichloromethane, a tan solid was obtained, weighing 3.24 g (37%); m.p. 101–103 °C. $^1$H NMR (300 MHz, [D$_6$]DMSO): $\delta$ = 7.77 (dd, $J$ = 7.5, 4.7 Hz, 2 H, Ar$H$), 7.59 (m, 1 H), 5.72 (t, $J$ = 5.5 Hz, 1 H, O$H$), 4.91 (d, $J$ = 5.2 Hz, 2 H, C$H_2$OH) ppm. $^{13}$C NMR (75 MHz, [D$_6$]DMSO): $\delta$ = 139.3, 139.2, 136.4, 133.2, 131.2, 128.4, 125.4, 120.7, 57.7 ppm. UV/Vis: $\lambda$ ($\varepsilon$, M$^{-1}$cm$^{-1}$) = 369 (3400), 352 (3800), 334 (2200) sh, 321 (1200) sh, 285 (5700), 275 (14000), 268 (13000) sh, 246 (14000), 239 (12000) nm. IR: $\tilde{\nu}$ = 3327, 3045, 2922, 1724, 1608 cm$^{-1}$. LRMS (EI, 70 eV, $m/z$): 268 [M]$^+$. $C_{16}H_{12}O_2S{\cdot}H_2O$ (286.3): calcd. C 67.11, H 4.93; found C 67.56, H 4.55.

**2a:** Compound **1a** (0.05 g, 0.25 mmol) was dissolved in chloroform (20 mL), and $MnO_2$ (0.325 g, 3.74 mmol) was then added. The dark black solution was stirred for 90 min and filtered through Celite. Slow evaporation of the solvent yielded colourless crystals weighing 0.049 g (99%); m.p. 132–134 °C. $^1$H NMR (300 MHz, CDCl$_3$): $\delta$ = 10.10 (s, 1 H, C$H$O), 2.94 (q, $J$ = 7.5 Hz, 2 H, C$H_2$CH$_3$), 1.25 (t, $J$ = 7.6 Hz, 3 H, CH$_2$C$H_3$) ppm. $^{13}$C NMR (75 MHz, CDCl$_3$): $\delta$ = 183.2, 152.1, 143.5, 19.8, 16.6 ppm. UV/Vis: $\lambda$ ($\varepsilon$, M$^{-1}$cm$^{-1}$) = 325 (5300) sh, 305 (7500), 230 (6300), 207 (18000) nm. IR: $\tilde{\nu}$ 2973 (CH), 2935 (CH), 2866 (CH), 2357 (CH), 1651 (CO), 702 (CS) cm$^{-1}$. LRMS (EI, 70 eV, $m/z$): 196.1 [M]$^+$. $C_{10}H_{12}O_2S$ (196.3): calcd. C 61.20, H 6.16; found C 60.93, H 6.45.

**2b:** Compound **1b** (0.3864 g, 1.3 mmol) was dissolved in chloroform (200 mL), and $MnO_2$ (1.700 g, 19.6 mmol) was then added. The dark black solution was stirred for 90 min and filtered through Celite. Slow evaporation of the solvent yielded colourless crystals weighing 0.3811 g (99%); m.p. 134–137 °C. $^1$H NMR (300 MHz, CDCl$_3$): $\delta$ = 9.79 (s, 1 H, C$H$O), 7.38–7.28 (m, 3 H), 7.16–7.09 (m, 2 H) ppm. $^{13}$C NMR (75 MHz, CDCl$_3$): $\delta$ = 185.2, 150.8, 144.1, 131.7, 130.5, 128.9, 128.5 ppm. UV/Vis: $\lambda$ ($\varepsilon$, M$^{-1}$cm$^{-1}$) = 348 (1900) sh, 315 (4000), 247 (6500), 208 (18000) nm. IR: $\tilde{\nu}$ = 3082 (CH), 3024 (CH), 2923 (CH), 1668 (CO), 1157 (CH), 697 (CS) cm$^{-1}$. LRMS (EI, 70 eV, $m/z$): 292.1 [M]$^+$. $C_{18}H_{12}O_2S$ (292.1): calcd. C 73.95, H 4.14; found C 73.55, H 4.10.

**2c:** Compound **1c** (0.0068 g, 0.025 mmol) was dissolved in THF (200 mL), and $MnO_2$ (0.033 g, 0.38 mmol) was then added. The dark black solution was stirred for 90 min and filtered through Celite. Slow evaporation of the solvent yielded red crystals weighing 0.0064 g (96%); m.p. 121–125 °C. $^1$H NMR (400 MHz, CDCl$_3$): $\delta$ = 10.35 (s, 1 H, C$H$O), 8.46 (d, $J$ = 7.1 Hz, 1 H, Ar$H$), 8.02 (d, $J$ = 8.2 Hz, 1 H, Ar$H$), 7.74 (dd, $J$ = 7.2, 8.2 Hz, 1 H, Ar$H$) ppm. $^{13}$C NMR (101 MHz, CDCl$_3$): $\delta$ = 182.0, 149.5, 136.3, 130.8, 130.6, 129.0, 128.3, 125.3 ppm. UV/Vis: $\lambda$ ($\varepsilon$, M$^{-1}$cm$^{-1}$) = 378 (8700), 331 (61000), 318 (39000) sh, 285 (15000), 238 (91000) nm. IR: $\tilde{\nu}$ = 3049 (CH), 2921 (CH), 2859 (CH), 1940 (CH), 1880 (CH), 1819 (CH), 1674 (CO), 770 (CS) cm$^{-1}$. LRMS (EI, 70 eV, $m/z$): 264.1 [M]$^+$. HRMS (EI, 70 eV, $m/z$): calcd. for $C_{15}H_8OS$ 236.0296 [M + OCH + H]$^+$; found 236.0296.

**3a:** Compound **2a** (0.100g, 0.51 mmol) was dissolved in absolute ethanol/THF (25 mL, 1:5), malononitrile (0.0741 g, 1.12 mmol) was added, and the mixture was gently heated to produce a yellow precipitate within 3 min. The solution was allowed to stir for an additional 20 min, and the precipitate was collected by vacuum filtration and washed with ethanol. Orange crystals were formed by recrystallisation from methanol/dichloromethane/toluene (10:10:1); yield 0.108 g, 72%; m.p. 231–233 °C. $^1$H NMR (400 MHz, CDCl$_3$): $\delta$ = 7.96 (s, 1 H, vinylC$H$), 2.81 (q, $J$ = 7.7 Hz, 2 H, C$H_2$CH$_3$), 1.24 (t, $J$ = 7.7 Hz, 3 H, CH$_2$C$H_3$) ppm. $^{13}$C NMR (101 MHz, CDCl$_3$): $\delta$ = 154.0, 147.1, 136.3, 113.5, 112.2, 82.5, 20.7, 16.4 ppm. UV/Vis: $\lambda$ ($\varepsilon$, M$^{-1}$cm$^{-1}$) = 438 (17000), 416 (19000), 392 (15000) sh, 372 (12000) sh, 284 (18000), 276 (16000), 210 (37000) nm. IR: $\tilde{\nu}$ = 3132, 3039, 2985, 2929, 2897, 2360, 2322, 2227 cm$^{-1}$. HRMS (EI, 70 eV, $m/z$): calcd. for $C_{16}H_{12}N_4S$ 292.0783 [M]$^+$; found 292.0791.

**3b:** Compound **2b** (0.100 g, 0.34 mmol) was dissolved in absolute ethanol/THF (25 mL, 1:5), and malononitrile (0.04971 g, 0.753 mmol) was added. The colourless solution was gently warmed to produce a bright yellow precipitate within 30 min. The precipitate was collected by vacuum filtration and washed with ethanol. Yellow crystals were formed by recrystallisation from methanol/dichloromethane/toluene (10:10:1); yield 0.089 g, 67%; m.p. 309–311 °C. $^1$H NMR (400 MHz, CDCl$_3$): $\delta$ = 7.70 (d, $J$ = 6.7 Hz, 1 H, vinylC$H$), 7.47–7.34 (m, 3 H), 7.00 (dd, $J$ = 1.3, 8.1 Hz, 2 H, Ar$H$) ppm. $^{13}$C NMR (101 MHz, [D$_8$]THF): $\delta$ = 149.8, 147.3, 130.5, 128.8, 127.1, 126.6, 111.4, 110.6, 81.4 ppm. UV/Vis: $\lambda$ ($\varepsilon$, M$^{-1}$cm$^{-1}$) = 434 (14248), 412 (16983), 391 (14649) sh, 305 (13266), 274 (19002), 237 (27506) sh, 209 (72269) nm. IR: $\tilde{\nu}$ = 3124, 3061, 3028, 2954, 2223 cm$^{-1}$. HRMS (EI, 70 eV, $m/z$): calcd. for $C_{24}H_{12}N_4S$ 388.0783 [M]$^+$; found 388.0784.

  

**3c:** Compound **2c** (0.05 g, 0.189 mmol) was dissolved in absolute ethanol/THF (25 mL, 1:5), and malononitrile (0.0275 g, 0.416 mmol) was added. The colourless solution was warmed and produced a dark red precipitate after 20 min, which was collected by vacuum filtration and washed with ethanol. The product was crystallised from methanol/dichloromethane/toluene (10:10:1); yield 0.0462 g, 68%; m.p. > 350 °C. $^1$H NMR (399 MHz, [D$_6$]-DMSO, 300 K): $\delta$ = 10.53 (s, 1 H, vinylC*H*), 9.18 (s, 1 H, vinylC*H*), 8.67 (d, $J$ = 7.2 Hz, 1 H, Ar*H*), 8.56 (d, $J$ = 7.0 Hz, 1 H, Ar*H*), 8.17 (d, $J$ = 8.2 Hz, 2 H, Ar*H*), 7.86–7.80 (m, 2 H) ppm. $^{13}$C NMR: the material was insufficiently soluble to acquire a spectrum. UV/Vis: $\lambda$ ($\varepsilon$, M$^{-1}$ cm$^{-1}$) = 491 (7600), 453 (10000), 381 (20000) sh, 358 (23000), 276 (11000), 251 (33000) sh, 244 (40000), 209 (103000) nm. IR: $\tilde{\nu}$ = 3082, 3034, 2900, 2831, 2229 cm$^{-1}$. HRMS (EI, 70 eV, *m*/*z*): calcd. for $C_{22}H_8N_4S$ 360.047 [M]$^+$; found 360.0473.

**4a:** Potassium *tert*-butoxide (0.0114 g, 0.102 mmol) was dissolved in absolute ethanol (3 mL). 2-Thiopheneacetonitrile (0.0628 g, 0.510 mmol) was added to the solution, and the mixture was allowed to stir at room temperature for an additional 30 min. In a separate flask, **2a** (0.05 g, 0.255 mmol) was dissolved in absolute ethanol/THF (4 mL, 3:1). The solution of **2a** was then added to the 2-thiopheneacetonitrile solution, and the mixture gave a red precipitate after 30 min of stirring at room temperature. The precipitate was collected by vacuum filtration and washed with ethanol. Red crystals were formed by recrystallisation from methanol/dichloromethane/toluene (10:10:1); yield 0.1005 g (97%); m.p. 241–242 °C. $^1$H NMR (400 MHz, $CDCl_3$): $\delta$ = 7.51 (s, 1 H, vinylC*H*), 7.38 (dd, $J$ = 1.0, 3.7 Hz, 1 H, Ar*H*), 7.30 (dd, $J$ = 1.0, 5.1 Hz, 1 H, Ar*H*), 7.08 (dd, $J$ = 3.7, 5.1 Hz, 1 H, Ar*H*), 2.75 (q, $J$ = 7.6 Hz, 2 H, C*H*$_2$CH$_3$), 1.21 (t, $J$ = 7.6 Hz, 3 H, CH$_2$C*H*$_3$) ppm. $^{13}$C NMR (100 MHz, $CDCl_3$): $\delta$ = 148.1, 139.5, 134.6, 129.0, 128.4, 127.5, 126.3, 116.6, 104.3, 20.5, 16.1 ppm. UV/Vis: $\lambda$ ($\varepsilon$, M$^{-1}$ cm$^{-1}$) = 491 (17400) sh, 458 (32000), 438 (30400) sh, 320 (10000), 317 (10200), 291 (7900) sh, 274 (4700) nm. IR: $\tilde{\nu}$ = 3448, 3080, 3030, 2974, 2935, 2877, 2210 cm$^{-1}$. LRMS (EI, 70 eV, *m*/*z*): $C_{22}H_{18}N_2S_3$ [M]$^+$ 406.0. $C_{22}H_{18}N_2S_3$ (406.1): calcd. C 64.99, H 4.46, N 6.89; found C 64.83, H 4.09, N 6.83.

**4b:** Potassium *tert*-butoxide (0.0077 g, 0.068 mmol) and 2-thiopheneacetonitrile (0.0438 g, 0.342 mmol) were dissolved in absolute ethanol (3 mL) and stirred for 15 min. In a separate flask, **2b** (0.050 g, 0.171 mmol) was dissolved in absolute ethanol/THF (4 mL, 2.5:1.5). The solution of **2b** was then added to the thiopheneacetonitrile mixture, and after 20 min, a reddish-orange precipitate was collected by vacuum filtration and washed with ethanol. Red crystals formed from methanol/dichloromethane/toluene (10:10:1); yield 0.081 g, 94%; m.p. 271–275 °C. $^1$H NMR (400 MHz, $CDCl_3$): $\delta$ = 7.35 (dd, $J$ = 0.9, 3.7 Hz, 1 H, Ar*H*), 7.34 (s, $J$ = 1.0 Hz, 1 H, vinylC*H*), 7.32 (m, 3 H), 7.25 (dd, $J$ = 1.0, 5.0 Hz, 1 H, Ar*H*), 7.06 (m, 3 H) ppm. $^{13}$C NMR (100 MHz, $CDCl_3$): $\delta$ = 146.9, 139.2, 135.6, 133.8, 130.7, 130.6, 128.3, 128.2, 128.2, 127.6, 126.6, 116.5, 105.4 ppm. UV/Vis: $\lambda$ ($\varepsilon$, M$^{-1}$ cm$^{-1}$) = 487 (20000) sh, 458 (32000), 437 (28000), 405 (15000), 343 (16000), 332 (16000), 286 (7600) nm. IR: $\tilde{\nu}$ = 3358, 3105, 3059, 3026, 2924, 2212 cm$^{-1}$. HRMS (EI, 70 eV, *m*/*z*): calcd. for $C_{30}H_{18}N_2S_3$ 502.0632 [M]$^+$; found 502.6723.

**4c:** Potassium *tert*-butoxide (0.0849 g, 0.757 mmol) and 2-thiopheneacetonitrile (0.0466 g, 0.378 mmol) were dissolved in absolute ethanol (3 mL) and stirred for 15 min. In a separate flask, **2c** (0.050 g, 0.189 mmol) was dissolved in absolute ethanol/THF (4 mL, 2.5:1.5). The solution of **2c** was then added to the thiopheneacetonitrile solution. Within 15 min, a dark red precipitate formed, which was collected by vacuum filtration and washed with ethanol. Red crystals were grown from methanol/dichloromethane/toluene (10:10:1); yield 0.0817 g, (91%); m.p. 342–344 °C. $^1$H NMR (399 MHz, [D$_6$]DMSO, 345 K): $\delta$ = 8.25 (s, 1 H, vinylC*H*), 8.15 (d, $J$ = 7.0 Hz, 1 H, Ar*H*), 8.03 (d, $J$ = 8.2 Hz, 1 H, Ar*H*), 7.82–7.75 (m, 2 H), 7.65 (d, $J$ = 3.7 Hz, 1 H, Ar*H*), 7.25 (t, $J$ = 4.4 Hz, 1 H, Ar*H*) ppm. $^{13}$C NMR: the material was not soluble enough to acquire a spectrum. UV/Vis: $\lambda$ ($\varepsilon$, M$^{-1}$ cm$^{-1}$) = 513 (17000), 479 (20000), 451 (14000) sh, 383 (22000), 368 (21000), 289 (8000), 254 (14000), 213 (37000) nm. IR: $\tilde{\nu}$ = 3427, 3109, 3068, 3028, 2926, 2852, 2212 cm$^{-1}$. HRMS (EI, 70 eV, *m*/*z*): calcd. for $C_{28}H_{14}N_2S_3$ 474.0319 [M]$^+$; found 474.0300.

**5a:** Compound **2a** (0.105 g, 0.534 mmol) was dissolved in dry dichloromethane (20 mL), and indole (0.263 g, 2.14 mmol) was added, followed by the quick addition of borontrifluoride–diethyl ether (0.0539 mL, 0.428 mmol). The flask was shielded from the light and stirred under an atmosphere of $N_2$. After 2 h, the solvent was removed in vacuo, and the residue was purified by column chromatography (silica gel, dichloromethane/methanol, 20:1), affording a dark red solid; yield 0.157 g, 47%; m.p. 191–193 °C. $^1$H NMR (399 MHz, [D$_6$]DMSO, 355 K): $\delta$ = 10.70 (s, 2 H, N*H*), 8.31 (s, 2 H, N*H*), 7.69–6.86 (m, 19 H), 6.33 (s, 1 H), 2.76 (q, $J$ = 7.4 Hz, 2 H, C*H*$_2$CH$_3$), 2.33 (q, $J$ = 7.5 Hz, 2 H, C*H*$_2$CH$_3$), 1.09 (t, $J$ = 7.4 Hz, 3 H, CH$_2$C*H*$_3$), 0.90 (t, $J$ = 7.5 Hz, 3 H, CH$_2$C*H*$_3$) ppm. $^{13}$C NMR (100 MHz, [D$_6$]DMSO, 355 K): $\delta$ = 137.2, 131.9, 128.4, 126.9, 126.0, 125.3, 124.4, 122.9, 122.0, 121.6, 121.3, 120.99, 119.2, 119.1, 117.8, 117.4, 112.3, 112.1, 67.5, 31.0, 25.6 ppm. UV/Vis: $\lambda$ ($\varepsilon$, M$^{-1}$ cm$^{-1}$) 508 (17000), 458 (19000), 388 (10000) sh, 290 (23000) sh, 282 (26000), 250 (29000), 229 (57000) nm. IR: $\tilde{\nu}$ = 3633, 3412, 3059, 2966, 2929, 2872 cm$^{-1}$. HRMS (TOF-MS, *m*/*z*): calcd. for $C_{42}H_{34}N_4S$ 627.2522 [M + H]$^+$; found 627.2546.

**5b:** Compound **2b** (0.100 g, 0.345 mmol) was dissolved in dry dichloromethane (20 mL), and indole (0.194 g, 1.66 mmol) was added, followed by the quick addition of borontrifluoride–diethyl ether (0.1824 mL, 1.45 mmol). The flask was shielded from the light and stirred under an atmosphere of $N_2$. After 2 h, the solvent was removed in vacuo, and the residue was purified by column chromatography (silica gel, dichloromethane/methanol, 20:1) affording a dark red solid; yield 0.122 g, 49%; m.p. > 350 °C. $^1$H NMR (399 MHz, [D$_6$]DMSO): $\delta$ = 10.95 (s, 1 H), 8.24 (s, 1 H), 7.58–6.57 (m, 31 H), 6.04 (s, 1 H) ppm. $^{13}$C NMR (101 MHz, [D$_6$]-DMSO): $\delta$ = 141.2, 137.1, 135.6, 135.1, 134.6, 130.3, 130.0, 129.9, 128.7, 127.9, 127.7, 127.4, 127.0, 126.4, 125.7, 124.3, 124.0, 123.6, 121.7, 121.2, 119.1, 119.1, 117.5, 115.3, 115.3 ppm. UV/Vis: $\lambda$ ($\varepsilon$, M$^{-1}$ cm$^{-1}$) = 522 (11000), 458 (14000), 340 (6000), 281 (24000), 242 (28000) nm. IR: $\tilde{\nu}$ = 3635, 3417, 3057, 2926, 1409 cm$^{-1}$. HRMS (EI, 70 eV, *m*/*z*): calcd. for $C_{50}H_{34}N_4S$ 722.2504 [M]$^+$; found 722.2485.

**5c:** Compound **2c** (0.016 g, 0.061 mmol) was dissolved in dry dichloromethane (8 mL), and indole (0.030 g, 0.254 mmol) was added, followed by the quick addition of borontrifluoride–diethyl ether (0.0345 mL, 0.243 mmol). The flask was shielded from the light and stirred under an atmosphere of $N_2$. After 2 h, the solvent was removed in vacuo, and the residue was directly purified by column chromatography [silica gel, dichloromethane/methanol (20:1)] affording a dark purple solid; yield 0.017 g, 41%; m.p. > 350 °C. $^1$H NMR (399 MHz, [D$_6$]DMSO, 370 K): $\delta$ = 8.34 (s, 1 H), 8.00–6.80 (m, 14 H) ppm. $^{13}$C NMR: the material was not soluble enough to acquire a spectrum. UV/Vis: $\lambda$ ($\varepsilon$, M$^{-1}$ cm$^{-1}$) = 602 (1500), 539 (4000) sh, 462 (9000), 385 (12000), 324 (17000), 277 (33000) sh, 245 (46000) nm. IR: $\tilde{\nu}$ = 3404, 3109, 3057, 2924, 2870, 1483, 1415 cm$^{-1}$. HRMS (TOF-MS, *m*/*z*): calcd. for $C_{48}H_{30}N_4S$ 695.2269 [M + H]$^+$; found 695.2237.

  

**Supporting Information** (see also the footnote on the first page of this article): $^{1}H$ and $^{13}C$ NMR spectra for **1**–**5**, a crystal comparison Table for **1b** and **2a**–**c**, the crystallographic packing for **1b**, **2a**–**c**, and **3a**,**b**, the computational data for **1**–**5**, the FMOs of **1**–**5**, UV/Vis spectra of **1a**–**c**, **3** and **4**, cyclic voltammetry of **1**–**4**, solution fluorescence spectra of **3c**, **4b**, **4c**, **5b** and **5c**, and solid-state fluorescence of **3a**, **3b** and **4**.

CCDC-695325 (for **1b**), -695326 (for **2a**), -695327 (for **2b**), -695328 (for **2c**), -735357 (for **3a**), -735358 (for **3b**) and -735359 (for **4a**) contain the supplementary crystallographic data for this paper. These data can be obtained free of charge via www.ccdc.cam.ac.uk/data_request/cif.

## Acknowledgments

The authors thank the Natural Sciences and Engineering Research Council of Canada, the Alberta Government and the Canadian Foundation for Innovation for funding.

[1] M.-C. Chen, Y.-J. Chiang, C. Kim, Y.-J. Guo, S.-Y. Chen, Y.-J. Liang, Y.-W. Huang, T.-S. Hu, G.-H. Lee, A. Facchetti, T. J. Marks, *Chem. Commun.* **2009**, 1846–1848.
[2] R. P. Ortiz, J. Casado, V. Hernandez, J. T. L. Navarrete, J. A. Letizia, M. A. Ratner, A. Facchetti, T. J. Marks, *Chem. Eur. J.* **2009**, *15*, 5023–5039.
[3] H. Usta, A. Facchetti, T. J. Marks, *J. Am. Chem. Soc.* **2008**, *130*, 8580–8581.
[4] H. Usta, C. Risko, Z. Wang, H. Huang, M. K. Deliomeroglu, A. Zhukhovitskiy, A. Facchetti, T. J. Marks, *J. Am. Chem. Soc.* **2009**, *131*, 5586–5608.
[5] M.-H. Yoon, S. A. DiBenedetto, A. Facchetti, T. J. Marks, *J. Am. Chem. Soc.* **2005**, *127*, 1348–1349.
[6] J. L. Segura, N. Martin, *J. Mater. Chem.* **2000**, *10*, 2403–2435.
[7] M. Muccini, *Nat. Mater.* **2006**, *5*, 605–613.
[8] H. Usta, A. Facchetti, T. J. Marks, *Org. Lett.* **2008**, *10*, 1385–1388.
[9] C. Kim, A. Facchetti, T. J. Marks, *Science* **2007**, *318*, 76–80.
[10] P. Gao, D. Beckmann, H. N. Tsao, X. Feng, V. Enkelmann, M. Baumgarten, W. Pisula, K. Muellen, *Adv. Mater.* **2009**, *21*, 213–216.
[11] M. Surin, P. Sonar, A. C. Grimsdale, K. Muellen, S. De Feyter, S. Habuchi, S. Sarzi, E. Braeken, A. Ver Heyen, M. Van der Auweraer, F. C. De Schryver, M. Cavallini, J.-F. Moulin, F. Biscarini, C. Femoni, R. Lazzaroni, P. Leclere, *J. Mater. Chem.* **2007**, *17*, 728–735.
[12] P. Gao, X. Feng, X. Yang, V. Enkelmann, M. Baumgarten, K. Muellen, *J. Org. Chem.* **2008**, *73*, 9207–9213.
[13] M. Segal, M. Singh, K. Rivoire, S. Difley, T. Van Voorhis, M. A. Baldo, *Nat. Mater.* **2007**, *6*, 374–378.
[14] I. F. Perepichka, D. F. Perepichka, H. Meng, F. Wudl, *Adv. Mater.* **2005**, *17*, 2281–2305.
[15] S. Cho, J. Yuen, J. Y. Kim, K. Lee, A. J. Heeger, *Appl. Phys. Lett.* **2006**, *89*, 153505/153501–153505/153503.
[16] C. Yang, S. Cho, R. C. Chiechi, W. Walker, N. E. Coates, D. Moses, A. J. Heeger, F. Wudl, *J. Am. Chem. Soc.* **2008**, *130*, 16524–16526.
[17] J. Pei, W.-L. Yu, W. Huang, A. J. Heeger, *Macromolecules* **2000**, *33*, 2462–2471.
[18] A. G. MacDiarmid, *Synth. Met.* **2001**, *125*, 11–22.
[19] Y. Shirota, *J. Mater. Chem.* **2000**, *10*, 1–25.
[20] L. M. Campos, A. Tontcheva, S. Guenes, G. Sonmez, H. Neugebauer, N. S. Sariciftci, F. Wudl, *Chem. Mater.* **2005**, *17*, 4031–4033.
[21] N. Armaroli, V. Balzani, *Angew. Chem. Int. Ed.* **2007**, *46*, 52–66.
[22] J. Dai, X. Jiang, H. Wang, D. Yan, *Appl. Phys. Lett.* **2007**, *91*, 253503/253501–253503/253503.
[23] A. Dhanabalan, J. K. J. Van Duren, P. A. Van Hal, J. L. J. Van Dongen, R. A. J. Janssen, *Adv. Funct. Mater.* **2001**, *11*, 255–262.
[24] P.-T. Wu, F. S. Kim, R. D. Champion, S. A. Jenekhe, *Macromolecules* **2008**, *41*, 7021–7028.
[25] L. R. Dalton, *Handbook of Conducting Polymers* (3rd Edition) **2007**, vol. 2, p. 6/1–6/39.
[26] J. Gierschner, J. Cornil, H.-J. Egelhaaf, *Adv. Mater.* **2007**, *19*, 173–191.
[27] A. Kohler, J. S. Wilson, R. H. Friend, *Adv. Mater.* **2002**, *14*, 701–707.
[28] U. Mitschke, P. Bauerle, *J. Mater. Chem.* **2000**, *10*, 1471–1507.
[29] D. F. Perepichka, M. R. Bryce, *Angew. Chem. Int. Ed.* **2005**, *44*, 5370–5373.
[30] H. S. Cho, D. H. Jeong, S. Cho, D. Kim, Y. Matsuzaki, K. Tanaka, A. Tsuda, A. Osuka, *J. Am. Chem. Soc.* **2002**, *124*, 14642–14654.
[31] A. Tsuda, H. Furuta, A. Osuka, *J. Am. Chem. Soc.* **2001**, *123*, 10304–10321.
[32] M. Ocafrain, T. K. Tran, P. Blanchard, S. Lenfant, S. Godey, D. Vuillaume, J. Roncali, *Adv. Funct. Mater.* **2008**, *18*, 2163–2171.
[33] F. Moggia, F. Fages, H. Brisset, C. Chaix, B. Mandrand, E. Levillain, J. Roncali, *J. Electroanal. Chem.* **2009**, *626*, 42–46.
[34] L. Pouchain, O. Aleveque, Y. Nicolas, A. Oger, C.-H. Le Regent, M. Allain, P. Blanchard, J. Roncali, *J. Org. Chem.* **2009**, *74*, 1054–1064.
[35] M. Bendikov, F. Wudl, D. F. Perepichka, *Chem. Rev.* **2004**, *104*, 4891–4946.
[36] R. J. Mullins, D. R. Williams, *Name React. Heterocycl. Chem.* **2005**, 199–206.
[37] H. Wynberg, D. J. Zwanenburg, *J. Org. Chem.* **1964**, *29*, 1919–1922.
[38] R. A. Aitken, A. N. Garnett, *J. Chem. Soc. Perkin Trans. 1* **2000**, 3020–3021.
[39] F. Banishoeib, A. Henckens, S. Fourier, G. Vanhooyland, M. Breselge, J. Manca, T. J. Cleij, L. Lutsen, D. Vanderzande, L. H. Nguyen, H. Neugebauer, N. S. Sariciftci, *Thin Solid Films* **2008**, *516*, 3978–3988.
[40] G. Trippe, D. Canevet, F. Le Derf, P. Frere, M. Salle, *Tetrahedron Lett.* **2008**, *49*, 5452–5454.
[41] J. Nakayama, Y. Hasegawa, Y. Sugihara, A. Ishii, *Sulfur Lett.* **1999**, *22*, 131–140.
[42] R. Chandra, A. Sarkar, N. Biswas, *Proc. Indian Natl. Sci. Acad. Part A* **1994**, *60*, 465–470.
[43] S. V. Ley, S. C. Smith, P. R. Woodward, *Tetrahedron* **1992**, *48*, 1145–1174.
[44] M. Bourgeaux, W. G. Skene, *J. Org. Chem.* **2007**, *72*, 8882–8892.
[45] S. Destri, M. Pasini, C. Pelizzi, W. Porzio, G. Predieri, C. Vignali, *Macromolecules* **1999**, *32*, 353–360.
[46] E. H. Elandaloussi, P. Frere, P. Richomme, J. Orduna, J. Garin, J. Roncali, *J. Am. Chem. Soc.* **1997**, *119*, 10774–10784.
[47] A. K. Mohanakrishnan, M. V. Lakshmikantham, M. P. Cava, R. D. Rogers, L. M. Rogers, *Tetrahedron* **1998**, *54*, 7075–7080.
[48] Y. Shimizu, Z. Shen, S. Ito, H. Uno, J. Daub, N. Ono, *Tetrahedron Lett.* **2002**, *43*, 8485–8488.
[49] Y. Shimizu, Z. Shen, T. Okujima, H. Uno, N. Ono, *Chem. Commun.* **2004**, 374–375.
[50] H. Uoyama, K. Nakamura, M. Tukiji, M. Furukawa, H. Uno, *Heterocycles* **2007**, *73*, 673–688.
[51] P. v. R. Schleyer, C. Maerker, A. Dransfeld, H. Jiao, N. J. R. v. E. Hommes, *J. Am. Chem. Soc.* **1996**, *118*, 6317–6318.
[52] L. Wang, H. J. Wang, W. B. Dong, Q. Y. Ge, L. Lin, *Struct. Chem.* **2007**, *18*, 25–31.
[53] M. J. Frisch, G. W. Trucks, H. B. Schlegel, G. E. Scuseria, M. A. Robb, J. R. Cheeseman, J. A. Montgomery, T. V. K. N. Kudin Jr., J. C. Burant, J. M. Millam, S. S. Iyengar, J. Tomasi, V. Barone, B. Mennucci, M. Cossi, G. Scalmani, N. Rega, G. A. Petersson, H. Nakatsuji, M. Hada, M. Ehara, K. Toyota, R.

  

Fukuda, J. Hasegawa, M. Ishida, T. Nakajima, Y. Honda, O. Kitao, H. Nakai, M. Klene, X. Li, J. E. Knox, H. P. Hratchian, J. B. Cross, V. Bakken, C. Adamo, J. Jaramillo, R. Gomperts, R. E. Stratmann, O. Yazyev, A. J. Austin, R. Cammi, C. Pomelli, J. W. Ochterski, P. Y. Ayala, K. Morokuma, G. A. Voth, P. Salvador, J. J. Dannenberg, V. G. Zakrzewski, S. Dapprich, A. D. Daniels, M. C. Strain, O. Farkas, D. K. Malick, A. D. Rabuck, K. Raghavachari, J. B. Foresman, J. V. Ortiz, Q. Cui, A. G. Baboul, S. Clifford, J. Cioslowski, B. B. Stefanov, G. Liu, A. Liashenko, P. Piskorz, I. Komaromi, R. L. Martin, D. J. Fox, T. Keith, M. A. Al-Laham, C. Y. Peng, A. Nanayakkara, M. Challacombe, P. M. W. Gill, B. Johnson, W. Chen, M. W. Wong, C. Gonzalez, J. A. Pople, *Gaussian 03*, Revision E.01, Gaussian, Inc., Wallingford, CT, **2004**.

[54] T. M. Pappenfus, B. J. Hermanson, T. J. Helland, G. G. W. Lee, S. M. Drew, K. R. Mann, K. A. McGee, S. C. Rasmussen, *Org. Lett.* **2008**, *10*, 1553–1556.

[55] P. Leriche, P. Frere, A. Cravino, O. Aleveque, J. Roncali, *J. Org. Chem.* **2007**, *72*, 8332–8336.

[56] H. Zimmer, K. Sudsuansri, H. B. Mark, B. Ziegler, *Phosphorus Sulfur Silicon Relat. Elements* **1997**, *122*, 269–286.

[57] A. F. Diaz, J. Crowley, J. Bargon, G. P. Gardini, J. B. Torrance, *J. Electroanal. Chem. Interfacial. Electrochem.* **1981**, *121*, 355–361.

[58] D. Jones, M. Guerra, L. Favaretto, A. Modelli, M. Fabrizio, G. Distefano, *J. Phys. Chem.* **1990**, *94*, 5761–5766.

[59] H. A. Ho, H. Brisset, E. H. Elandaloussi, P. Frère, J. Roncali, *Adv. Mater.* **1996**, *8*, 990–994.

[60] J. Roncali, *Macromol. Rapid Commun.* **2007**, *28*, 1761–1775.

[61] T. Sone, *Bull. Chem. Soc. Jpn.* **1964**, *37*, 1197–1200.

[62] D. Lorcy, K. D. Robinson, Y. Okuda, J. L. Atwood, M. P. Cava, *J. Chem. Soc., Chem. Commun.* **1993**, 345–347.

[63] M. Scholz, G. Gescheidt, U. Schoeberl, J. Daub, *J. Chem. Soc. Perkin Trans. 2* **1992**, 2137–2143.

[64] H. A. Ho, H. Brisset, E. H. Elandaloussi, P. Frere, J. Roncali, *Adv. Mater.* **1996**, *8*, 990–994.

[65] U. Schlick, F. Teichert, M. Hanack, *Synth. Met.* **1998**, *92*, 75–85.

[66] G. Zotti, S. Zecchin, G. Schiavon, A. Berlin, G. Pagani, M. Borgonovo, R. Lazzaroni, *Chem. Mater.* **1997**, *9*, 2876–2886.

[67] P. Wagner, D. L. Officer, M. Kubicki, *Acta Crystallogr., Sect. E: Struct. Rep. Online* **2006**, *62*, o5931–o5932.

[68] S. Echinger, U. Schmid, F. Teichert, J. Hieber, H. Ritter, M. Hanack, *Synth. Met.* **1993**, *61*, 163–165.

[69] M. Hanack, G. Hieber, K. M. Mangold, H. Ritter, U. Roehrig, U. Schmid, *Synth. Met.* **1993**, *55*, 827–832.

[70] M. Hanack, K.-M. Mangold, U. Roehrig, C. Maichle-Moessmer, *Synth. Met.* **1993**, *60*, 199–210.

[71] H. Ritter, K. M. Mangold, U. Roehrig, U. Schmid, M. Hanack, *Synth. Met.* **1993**, *55*, 1193–1197.

[72] A. Ishii, Y. Horikawa, I. Takaki, J. Shibata, J. Nakayama, M. Hoshino, *Tetrahedron Lett.* **1991**, *32*, 4313–4316.

[73] S. Ito, S. Kikuchi, T. Okujima, N. Morita, T. Asao, *J. Org. Chem.* **2001**, *66*, 2470–2479.

[74] S.-i. Takekuma, K. Sonoda, T. Minematsu, H. Takekuma, *Tetrahedron* **2008**, *64*, 3802–3812.

Received: July 27, 2009
Published Online: September 21, 2009

  